IN-39
8224
P12

NASA Technical Memorandum 104048

ACTIVE VIBRATION ABSORBER FOR CSI EVOLUTIONARY MODEL: DESIGN AND EXPERIMENTAL RESULTS

Anne M. Bruner, W. Keith Belvin, Lucas G. Horta, and Jer-Nan Juang

(NASA-TM-104048) ACTIVE VIBRATION ABSORBER FOR CSI EVOLUTIONARY MODEL: DESIGN AND EXPERIMENTAL RESULTS (NASA) 12 p CSCL 20K
N91-21578
Unclas
G3/39 0008224

March 1991

NASA
National Aeronautics and
Space Administration

Langley Research Center
Hampton, Virginia 23665

ACTIVE VIBRATION ABSORBER FOR THE CSI EVOLUTIONARY MODEL: DESIGN AND EXPERIMENTAL RESULTS

Anne M. Bruner*
Lockheed Engineering and Sciences Company
Hampton, Virginia

W. Keith Belvin†, Lucas G. Horta† and Jer-Nan Juang**
NASA Langley Research Center
Hampton, Virginia

Abstract

The development of control of large flexible structures technology must include practical demonstrations to aid in the understanding and characterization of controlled structures in space. To support this effort, a testbed facility has been developed to study practical implementation of new control technologies under realistic conditions. The paper discusses the design of a second order, acceleration feedback controller which acts as an active vibration absorber. This controller provides guaranteed stability margins for collocated sensor/actuator pairs in the absence of sensor/actuator dynamics and computational time delay. Experimental results in the presence of these factors are presented and discussed. The primary performance objective considered is damping augmentation of the first nine structural modes. Comparison of experimental and predicted closed-loop damping is presented, including test and simulated time histories for open and closed-loop cases. Although the simulation and test results are not in full agreement, robustness of this design under model uncertainty is demonstrated. The basic advantage of this second-order controller design is that the stability of the controller is model independent.

Introduction

Large space structure control requires special control design methodology. High modal density in the controller bandwidth makes rolloff of control authority a problem. Many of the theoretical issues with regard to large space structure control were recognized and initially treated by Benhabid, Flashner, and Tung.[1] Experimental validation is now being demonstrated with a series of facilities which have been designed for that purpose.[2,3,4] It is recognized that the complexity of these structures foster the use of controllers with high and low authority. Theoretically, low authority controllers are used to augment the inherent damping of the structure, while the high authority controllers are designed to achieve the desired performance. One form of these low authority controllers is an active vibration absorber (AVA), which is the subject of this paper.

NASA and the Controls Structures Interaction (CSI) program have undertaken the design, development, and fabrication of generic structures to study fundamental problems in the implementation of advanced control methodologies. The program stresses the application of existing sensor and actuator technologies for identification and control. The first such testbed of the CSI program has been completed at the NASA Langley Research Center. The configuration selected, which is described in detail in a later section, uses thrusters and accelerometers as its primary actuation and sensing devices. Initially, controller designs that would not require knowledge of the dynamics of the structure are preferred. This allows the implementation of such controllers even when model uncertainties are large. For this purpose, a procedure for designing second order controllers using passitivity concepts is discussed for continuous time systems.[5] Using this approach, decentralized controllers have been designed and used for experimental validation.

The paper outline is as follows: first the controller design theory is presented followed by a mechanical analogy. A brief description of the testbed is given, and a controller design procedure for the laboratory model is described. Finally, test results from the experimental implementation are provided and compared with the analytical results.

---

* Structural Control Engineer, Lockheed Engineering and Sciences Company, Hampton, VA.

† Aerospace Engineer, Structural Dynamics Branch, Member AIAA.

** Principal Scientist, Structural Dynamics Branch, Associate Fellow AIAA.

Controller Design Theory

For large scale systems, a model of the structure is often obtained via finite element methods resulting in a set of state and output equations of the form:

$$M\ddot{z} + D\dot{z} + Kz = Bu \qquad (1)$$

$$y = H_a\ddot{z} + H_v\dot{z} + H_d z \qquad (2)$$

Here z is an $n \times 1$ state vector, and M, D, and K are mass, damping, and stiffness matrices, respectively, which generally are symmetric and sparse. The $n \times p$ influence matrix B describes the actuator force distributions for the $p \times 1$ input vector u. Equation (2) is a measurement equation with y as the $m \times 1$ measurement vector, H_a the $m \times n$ acceleration influence matrix, H_v the $m \times n$ velocity influence matrix, and H_d the $m \times n$ displacement influence matrix. For direct output feedback control, the input vector u can be written

$$u = -Gy = -GH_a\ddot{z} - GH_v\dot{z} - GH_d z \qquad (3)$$

where G is a gain matrix to be determined. Substituting Eq. (3) into Eq. (1) yields

$$(M + BGH_a)\ddot{z} + (D + BGH_v)\dot{z} + (K + BGH_d)z = 0 \quad (4)$$

It is shown by Juang and Phan[5] that for a structural system, output velocity feedback with collocated sensors and actuators makes the closed-loop system asymptotically stable with an infinite gain margin. Without velocity sensors, however, the system damping cannot be augmented with direct output feedback unless additional dynamics are introduced.

Let the controller to be designed have a set of second-order dynamic equations and measurement equations similar to the system equations, Eqs. (1) and (2),

$$M_c\ddot{z}_c + D_c\dot{z}_c + K_c z_c = B_c u_c \qquad (5)$$

$$y_c = H_{ac}\ddot{z}_c + H_{vc}\dot{z}_c + H_{dc} z_c \qquad (6)$$

Here z_c is the controller state vector of dimension n_c, and M_c, D_c, and K_c can be interpreted as the controller mass, damping, and stiffness matrices, respectively, which in general, are symmetric and positive definite to make the controller asymptotically stable. The $n_c \times m$ influence matrix B_c describes the force distributions for the $m \times 1$ input force vector u_c. Equation (6) is the controller measurement equation having y_c as the measurement vector of length p, H_{ac} the $p \times n_c$ acceleration influence matrix, H_{vc} the $p \times n_c$ velocity influence matrix, and H_{dc} the $p \times n_c$ displacement influence matrix. All the quantities u_c, y_c, and n_c, are arbitrary which means that M_c, D_c, K_c, H_{dc}, H_{vc}, H_{ac} and B_c are the design parameters for the controller.

Let the input vector u in Eq. (1) and u_c in Eq. (5) be

$$u = y_c = H_{ac}\ddot{z}_c + H_{vc}\dot{z}_c + H_{dc} z_c \qquad (7)$$

$$u_c = y = H_a\ddot{z} + H_v\dot{z} + H_d z \qquad (8)$$

Substituting Eq. (7) into Eq. (1) and Eq. (8) into Eq. (5) yields

$$M_t\ddot{z}_t + D_t\dot{z}_t + K_t z_t = 0 \qquad (9)$$

where

$$M_t = \begin{bmatrix} M & -BH_{ac} \\ -B_cH_a & M_c \end{bmatrix},$$

$$D_t = \begin{bmatrix} D & -BH_{vc} \\ -B_cH_v & D_c \end{bmatrix},$$

$$K_t = \begin{bmatrix} K & -BH_{dc} \\ -B_cH_d & K_c \end{bmatrix}, \quad z_t = \begin{bmatrix} z \\ z_c \end{bmatrix}$$

If the design parameters are chosen such that M_t, D_t and K_t are positive definite, the closed loop system, Eq. (9), becomes asymptotically stable.

Consider the special case for acceleration feedback only where $H_d = H_v = H_{dc} = H_{vc} = 0$ in Eq. (9). This makes the closed-loop mass, damping and stiffness matrices

$$M_t = \begin{bmatrix} M & -BH_{ac} \\ -B_cH_a & M_c \end{bmatrix}, \quad D_t = \begin{bmatrix} D & 0 \\ 0 & D_c \end{bmatrix},$$

$$K_t = \begin{bmatrix} K & 0 \\ 0 & K_c \end{bmatrix}$$

For M_t to be a positive definite matrix, it must be a real, symmetric matrix satisfying

$$z_t^T M_t z_t > 0 \qquad (10)$$

for any real vector z_t except the null vector. To make M_t symmetric, it is required that

$$BH_{ac} = H_a^T B_c^T \qquad (11)$$

Substituting the definition of z_t and M_t into Eq. (10) and using Eq. (11) yields

$$z_t^T M_t z_t = z^T(M - BH_{ac}H_{ac}^T B^T)z +$$

$$(H_{ac}^T B^T z - z_c)^T(H_{ac}^T B^T z - z_c) + z_c^T(M_c - I)z_c$$

This equation is greater than zero if H_{ac} and M_c are chosen such that $M - BH_{ac}H_{ac}^T B^T$ and $M_c - I$ are positive definite. Note that this is a sufficient condition but not a necessary one.

In an attempt to obtain a controller structure without this restriction on H_{ac} and M_c, let the u in Eq. (7) be modified to include a direct acceleration feedback term. Then

$$u = y_c - G_a y = H_{ac}\ddot{x}_c - G_a y \qquad (12)$$

which makes

$$M_t = \begin{bmatrix} M + BG_aH_a & -BH_{ac} \\ -B_cH_a & M_c \end{bmatrix} \qquad (13)$$

Defining

$$G_a = H_{ac}M_c^{-1}B_c \qquad (14)$$

substituting into Eq. (13), and using the symmetry condition in Eq. (11), the positive definite condition in Eq. (10) becomes

$$x_t^T M_t x_t = x^T M x +$$

$$(M_c^{-1}B_cH_a x - x_c)^T M_c (M_c^{-1}B_cH_a x - x_c) \qquad (15)$$

which is positive if M and M_c are positive definite matrices. Figure 1 shows a block diagram of the closed-loop system with acceleration feedback. Figure 2 depicts a reduced block diagram for the same system. To design a second-order controller having the structure given in (5),(6),(8),(12), and (14), it is only necessary to require M_c, D_c and K_c to be positive definite and that Eq. (11) is satisfied.

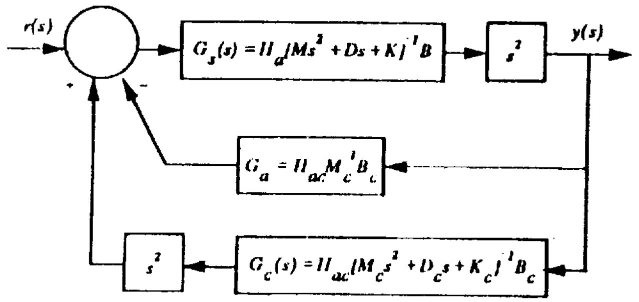
r(s)
+
−
G_s(s) = H_a[Ms² + Ds + K]⁻¹B
s²
y(s)
G_a = H_ac M_c⁻¹ B_c
s²
G_c(s) = H_ac[M_c s² + D_c s + K_c]⁻¹B_c

Figure 1. Block diagram of closed-loop system with direct and dynamic feedback

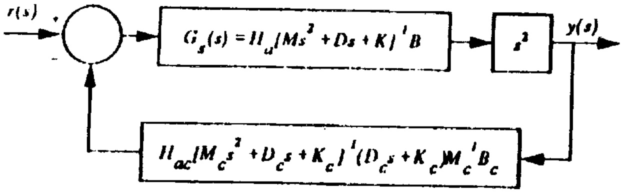
r(s)
+
−
G_s(s) = H_a[Ms² + Ds + K]⁻¹B
s²
y(s)
H_ac[M_c s² + D_c s + K_c]⁻¹(D_c s + K_c)M_c⁻¹B_c

Figure 2. Reduced block diagram of closed-loop system with general acceleration feedback

Mechanical Analogy

With further constraints on the plant and controller, this second-order controller can be thought of as attaching an additional mass, spring and damper assembly to the structure at the location of the sensors/actuators. For the case of a single mode plant, a diagram representing the closed-loop system can be drawn as shown in Fig. 3. Letting $x_c = x_a - x$ results in plant and controller equations:

$$Plant: M\ddot{x} + D\dot{x} + Kx = z_c$$

$$y = \ddot{x} \qquad (16)$$

$$Controller: M_c\ddot{x}_c + D_c\dot{x}_c + K_c x_c = -M_c y$$

$$z_c = -K_c x_c - D_c\dot{x}_c \qquad (17)$$

A block diagram for this physical system is shown in Fig. 4. Upon comparison of Fig. 2 and Fig. 4, H_{ac} and B_c must satisfy

$$H_{ac}B_c = M_c^2 \qquad (18)$$

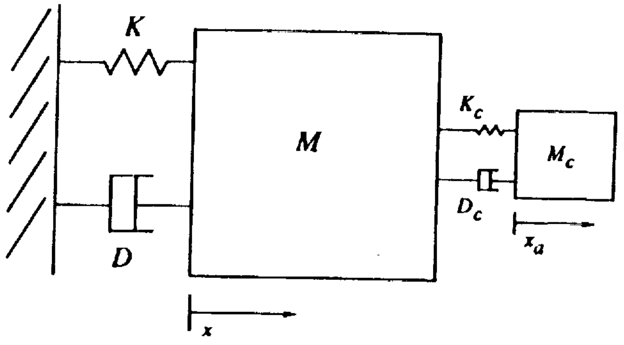

Figure 3. Single mode structure-controller design model

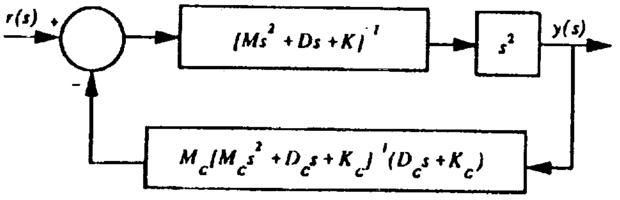

Figure 4. Block diagram of single mode structure controller closed-loop system

Assuming collocated sensors and actuators and unity force input, the constraints given in Eqs. (11) and (18) dictate:

$$H_a = 1 \tag{19}$$

$$B = 1 \tag{20}$$

$$H_{ac} = M_c \tag{21}$$

$$B_c = M_c \tag{22}$$

Using the controller equations given in Eq. (17), a state space model can be written:

$$\dot{\bar{z}} = A\bar{z} + By \tag{23}$$

$$u = C\bar{z} + Dy \tag{24}$$

where

$$A = \begin{bmatrix} 0 & 1 \\ K_c/M_c & -D_c/M_c \end{bmatrix}, \quad B = \begin{bmatrix} 0 \\ 1 \end{bmatrix},$$

$$C = [\,-K_c \quad -D_c\,], \quad D = [0], \quad \bar{z} = \begin{bmatrix} z_c \\ \dot{z}_c \end{bmatrix}$$

The controller low frequency gain equals M_c. In the presence of sensor bias, a large M_c could result in large actuator command offsets or even saturation. It is important to select conservative values for M_c to reduce the effects of offsets. In analogy with vibration absorbers[6], the frequency of the absorber is set equal to the targeted mode, i.e. $\omega^2 = K_c/M_c$. After selecting values for M_c and K_c, values for D_c are selected based on root locus design. In the following section, a description of the testbed facility is presented.

Laboratory Model Description

A photograph of the evolutionary model testbed [4] is shown in Fig. 5. The structure weighs 741 lbs. and is supported from the ceiling with two steel cables with lengths of 64.5 ft. each. The truss is made of aluminum struts forming 10 in. cube bays of single lace diagonals alternating so that opposite faces cross. The batten plane has diagonals which also alternate. The major components of the structure are the center section 52.5 ft. long, a 16 ft. diameter reflector, and a 9.2 ft. tower where a laser beam is located. The steel cables are attached to the ends of two cross member trusses 16.7 ft. long to ensure stability when suspended. The actuators are proportional thrusters using a 125 psi external air supply connected to the model via flexible rubber hoses. A total of 8 actuator pairs are placed at four locations along the truss as shown in Fig. 6, and each actuator pair is capable of producing 4.4 lbs. In addition, 8 accelerometers are located with the thrusters for identification and control experiments. The finite element model has 81 modes below 50 Hz. Because of the suspension, the first six structural modes are pendulum modes with frequencies between 0.1 Hz. and 0.9 Hz. The next three modes are bending modes with frequencies between 1.4 Hz and 1.9 Hz. Orthogonal views of the mode shapes for modes 6 through 9 are provided in Figs. 7-10. Control laws are implemented on a digital computer at sampling rates of 80 Hz and 350 Hz.

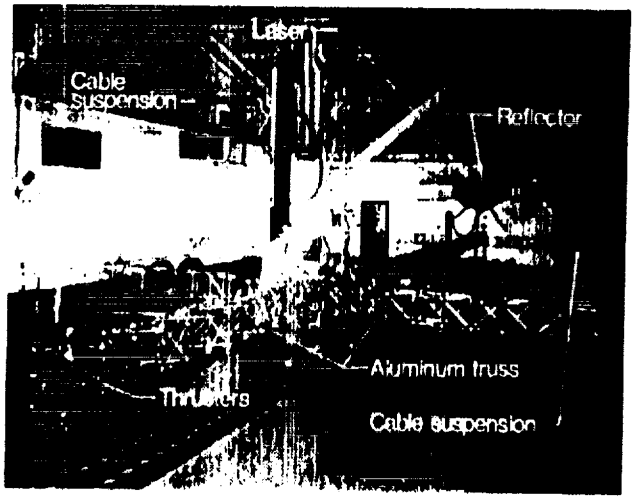

Figure 5. Photograph of the CSI Evolutionary Model testbed

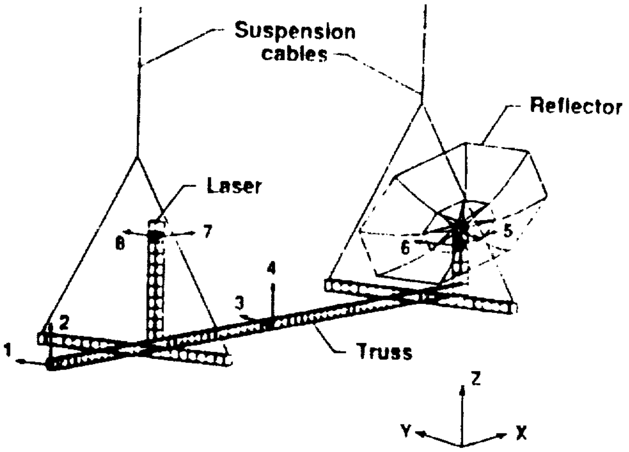

Figure 6. Schematic of the CSI Evolutionary Model showing actuator/sensor locations

ORIGINAL PAGE IS
OF POOR QUALITY

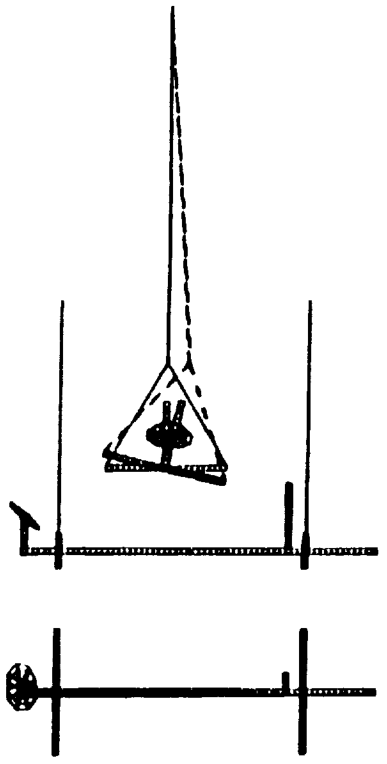

Figure 7. Vibration mode 6, f=0.9 Hz

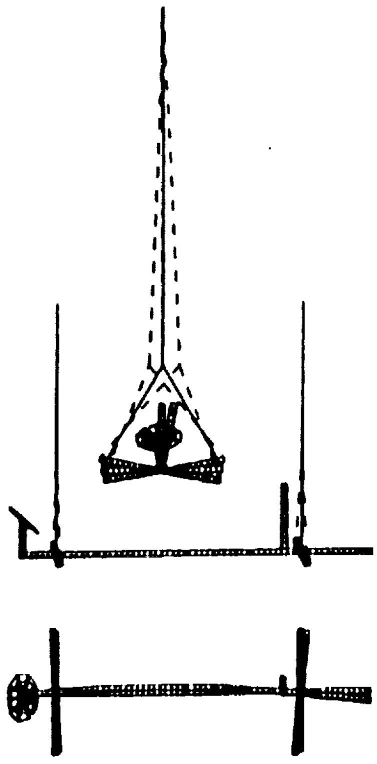

Figure 8. Vibration mode 7, f=1.4 Hz

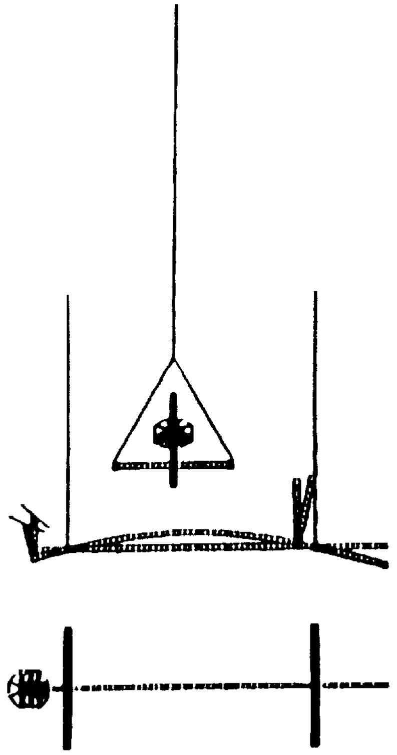

Figure 9. Vibration mode 8, f=1.7 Hz

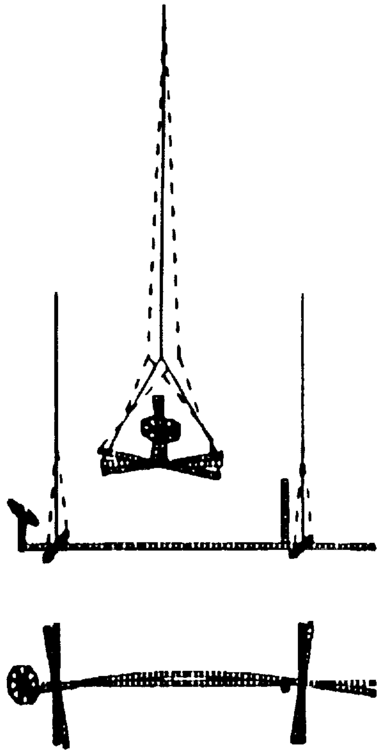

Figure 10. Vibration mode 9, f=1.9 Hz

ORIGINAL PAGE IS
OF POOR QUALITY

Controller Design

The design theory discussed is now used to develop SISO controllers for each actuator/sensor pair. The design approach is to determine the most controllable/observable mode(s) for a particular input/output pair and tune a second order controller to the mode(s). Each second order controller has three design parameters, namely, M_c, D_c, and K_c. If one actuator/sensor pair is to control n separated modes, n distinct sets of design parameters need to be determined. The procedure used to design controllers for the evolutionary model is the following:

(1) Choose M_c to avoid large command offsets.

(2) Choose a target mode for each actuator/sensor pair and determine the value of K_c needed to match its frequency, where $K_c/M_c = \omega^2$.

(3) Determine the value of D_c which optimizes the damping value of the target mode.

The design objective is to increase damping in the first nine modes. A value of 0.1 is selected for M_c based on previous experimental results. The modes selected and the corresponding actuator/sensor pair used to control them are presented in Table 1. Each actuator/sensor location is labeled with a number from 1 to 8, (see Fig. 6). Using Table 1, actuator/sensor pair at location 4 is responsible for controlling mode number 8. The actuators at locations 1,2,3, and 7 have two independent controllers for the 1^{st} and 2^{nd} target modes, while the remaining four have one. Although the actuator/sensor at location 8 is responsible for modes 6 and 7, only one controller is designed by tuning its frequency in between the two modes. To optimize damping, a root locus is performed for each actuator/sensor pair by fixing M_c and K_c and varying D_c. In locations where more than one controller is used, each controller is optimized separately. Figure 11 shows the root locus for mode 6 using actuator/sensor pair 8 for values of D_c ranging from 0.1 to 1.0. A maximum damping value of 3.5% is achieved when D_c=0.4. The controller parameter values, M_c, D_c, and K_c, for each second order controller designed are given in Table 2.

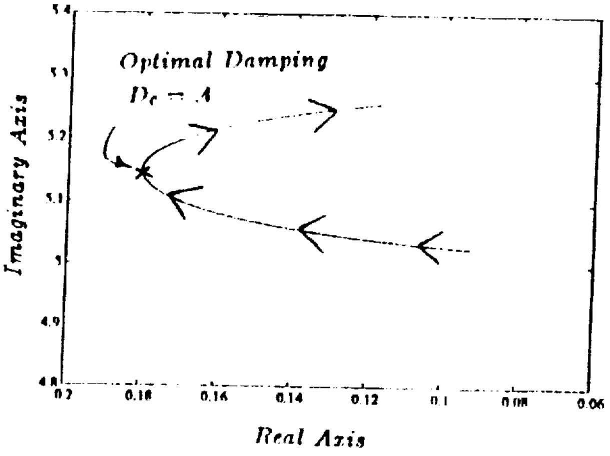

Figure 11. Mode 6 root locus with controller parameter D_c

Table 1: Mode number to be controlled and corresponding actuator/sensor location

Location No.	1^{st} Target Mode	2^{nd} Target Mode
1	3	9
2	4	8
3	2	9
4	8	-
5	1	-
6	3	-
7	1	8
8	6	7

Table 2: Controller design parameters

	1^{st} Target Mode			2^{nd} Target Mode		
Location	M_c	D_c	K_c	M_c	D_c	K_c
1	.1	.06	.089	.1	.4	13.22
2	.1	.2	2.10	.1	.5	10.88
3	.1	.04	.083	.1	.4	13.22
4	.1	.4	10.88	-	-	-
5	.1	.03	.083	-	-	-
6	.1	.04	.083	-	-	-
7	.1	.03	.083	.1	.4	10.88
8	.1	.4	3.95	-	-	-

ORIGINAL PAGE IS
OF POOR QUALITY

Experimental Results

I. Implementation Issues

The controllers described in the previous section have special properties that must be considered in the actual implementation. The active implementation of the AVA controller should ideally emulate a physical spring-mass-damper attached to a structure at a single point. This statement implies the critical assumption that collocated sensors and actuators can be realized in the active implementation of the controller. Sensor and actuator collocation must be spatial and temporal. Spatial collocation is difficult to achieve because of the finite dimensions of sensors and actuators. Typical mounting of sensors and actuators result in spatially close arrangements, not collocated. Temporal collocation is even more difficult to achieve. First, the sensors and actuators must have no inherent dynamics in the frequency range zero to infinity. Second, the control law calculation must produce no phase shift except for that produced by the AVA controller. Hence, temporal collocation can be most closely achieved with very large bandwidth sensors and actuators and analog computations.

In the following paragraphs, the digital implementation of the AVA controller will be demonstrated on the structure shown in Fig. 5. The effects of sample delay, the sequence of real time computations, and spatial non-collocation are shown using experimental data. It should be noted that the sensors used in this study have a bandwidth of 300 Hz, whereas the actuators have a bandwidth of about 45 Hz. In our case, the maximum frequency to be controlled is at 1.9 Hz, and thus, the assumption of negligible sensor and actuator dynamics is not grossly violated.

Figure 12 shows the closed-loop implementation of the system controller. The external disturbance r produces the structural acceleration output y. Switches A and B are used to close the controller loop. Classic implementation of Kalman filter based controllers call for switch A to be closed at all times since the controller is actually an estimator of the structural states. It will be shown that the AVA controller is not an estimator and switches A and B should be closed simultaneously to activate closed-loop control. When closed-loop control is activated the following steps take place at each of the k^{th} sample periods:

(1) Input $y(k)$

(2) Output $u(k)$

(3) Compute control force $u(k+1) = C\bar{z}(k) + Dy(k)$

(4) Compute controller states $\bar{z}(k+1) = \Phi\bar{z}(k) + \Gamma y(k)$

(5) Wait for next clock pulse

where Φ and Γ are the time discretized versions of the A and B matrices in Eq. (23). It is also noted that the D matrix for the AVA controller is null.

The AVA controller has been implemented following the sequence of steps above at a sample rate of 80 Hz. The structure was excited at two bending modes and two pendulum modes for 10 seconds, then closed-loop control was initiated at 12.5 seconds. Figure 13 shows the acceleration output with switch A closed from t=0 seconds and implementing steps 1-5 above in sequence. The controller is unstable in a mode near 7 Hz. Since the AVA controller is not an estimator, switch A and B were closed simultaneously at t=12.5 seconds in the test data of Fig. 14. Even though the controller is still unstable, the initial closed-loop acceleration is much improved. This is due to a smooth transition from open to closed-loop. To further improve the closed-loop behavior, the controller time delay should be reduced. This can be achieved by eliminating the full time step delay that occurs in the computations of steps 1-5 above. Since the D matrix is null, steps 3 and 4 may be reordered to compute the controller state first and then the control force. This eliminates the one step delay and results in a stable controller as shown in Fig. 15. Note that it is preferred to reorder the computing sequence instead of substituting the state equation into the control equation to eliminate time delay as the latter results in a D matrix which is not null thus requiring additional computations.

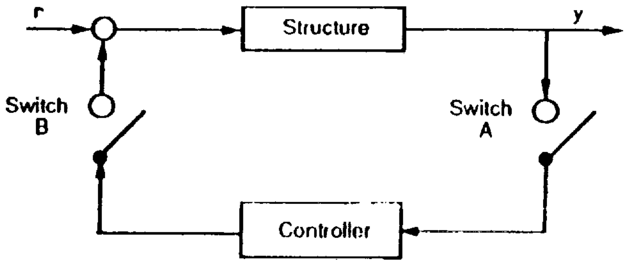

Figure 12. Controller closed-loop implementation

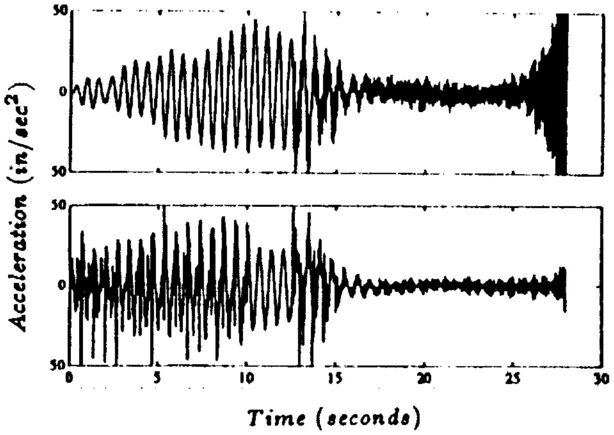

Figure 13. Closed-loop responses at locations 1 and 3 with switch A closed at t=0

ORIGINAL PAGE IS
OF POOR QUALITY

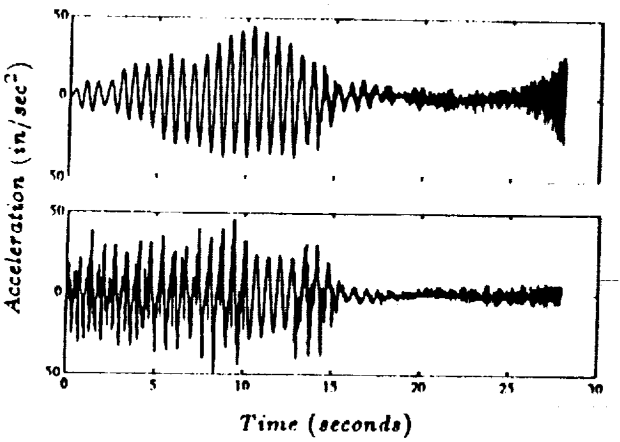

Figure 14. Closed-loop responses at locations 1 and 3 with switch A closed at t=12.5

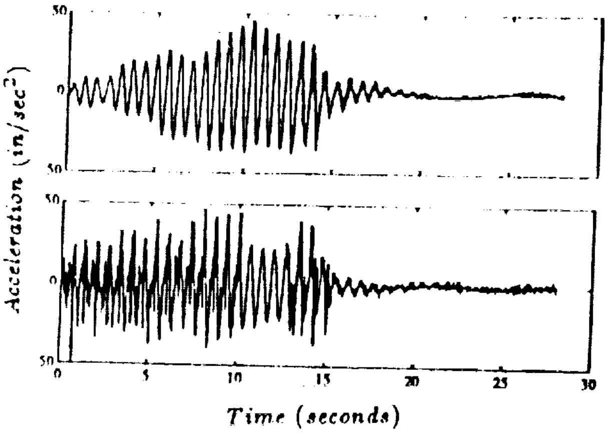

Figure 15. Closed loop responses at locations 1 and 3 without one step delay

Although the controller is now stable, the response indicates aliasing because of the relatively slow sample rate. When increasing the sample rate, the number of computations required to implement the controller is usually a limiting factor. Hence it is desirable to limit the size of the controller computations. This is often done by controller state reduction, or block diagonalization of the n by n state matrix Φ using some real transformation. An interesting feature of the AVA controller is its second-order structure. When transformed to a first order form, the second-order controller equations do not represent n independent states but rather $n/2$ independent states. This permits the controller rate states to be expressed in terms of controller position states. For example, a one-step implicit trapezoidal integration results in the rate states v as functions of the position states d as:

$$v(k) = \frac{2}{h}[d(k) - d(k-1)] - v(k-1)$$

where h is the time step, $h = t(k) - t(k-1)$. The above equation was used to reduce the controller state computations for the AVA controller which permitted a speed increase from 80 Hz to 350 Hz for the 24 state, 8-input 8-output controller using a VAXstation 3200 computer. Figure 16 shows the response of the system for this update rate. Notice the aliasing that occurred while sampling at 80 Hz is now absent and that the closed-loop performance is improved.

In Fig. 16 a 32 Hz mode is being excited by the controller that was not noticeably excited in the excitation phase. This 32 Hz mode has been traced to spatial non-collocation of the sensors and actuators in the original installation. Figure 17 shows the original installation has the actuators (thrusters) mounted in the center of the truss bay faces, whereas the sensors were mounted on the truss bay corners. Because of this spatial offset, torsion-bending coupling of the truss vibrations resulted in the closed-loop controller exciting a torsion mode at 32 Hz. The sensor installation was modified as shown in Fig. 17 to prevent local torsional behavior from being sensed.

This modified installation was used in the results of Fig. 18. As can be seen, the 32 Hz mode is no longer being driven by the controller.

In summary, the implementation of the AVA controller using acceleration feedback is improved by:

(a) Not calculating controller states during the excitation phase

(b) Resequencing the controller compute steps to reduce delay

(c) Updating the controller as fast as possible

(d) Improving the spatial collocation of sensors and actuators.

The following section will describe the controller performance shown in Fig. 18 in more detail.

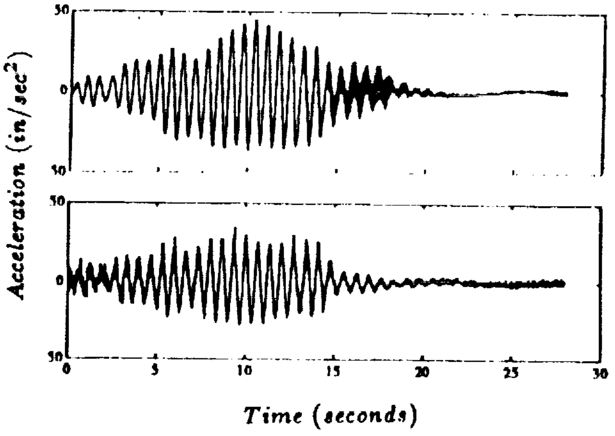

Figure 16. Closed-loop responses at locations 1 and 3 with 350 Hz sample rate

ORIGINAL PAGE IS
OF POOR QUALITY

II. Simulation and Test Comparison

In determining the success of AVA controller, each of the nine modes was excited independently, and the controller was then activated for vibration suppression. The top of Fig. 19 shows the experimental open and closed-loop accelerometer responses for the sixth mode of the structure. This mode is controlled from location 8. For open-loop, the structure is excited using sinusoidal excitation at the frequency of the mode of interest for the first 10 seconds. For closed-loop, the structure is excited in the same manner, and then the controller is activated for the duration of each test. Shown in the bottom of Fig. 19 are the open and closed-loop time history computer simulations performed for the same conditions. Figure 20 depicts the experimental and simulated open and closed-loop responses for the eighth mode.

Table 3 lists the finite element and experimental frequencies, open-loop damping, predicted closed-loop damping, and experimental closed-loop damping. The experimental and analytical frequencies for the first nine modes are fairly accurate, but at higher frequencies (not shown), this accuracy decreases considerably. The predicted and actual damping values achieved when implementing this controller are somewhat different. It is of interest to note that mode 2 showed no damping improvement in the experiment. This is due in part to the pendulum mode acceleration being nearly equal and opposite to the geometric change in acceleration due to gravity. Since the finite element model of the structure does not include gravity, the experimentally sensed acceleration for this mode is significantly lower than predicted. Although the damping obtained with the AVA controller is not predicted well, stability is conserved under modeling errors.

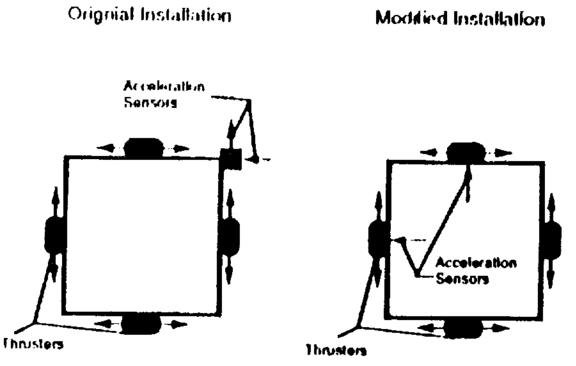

Figure 17. Testbed sensor/actuator installation

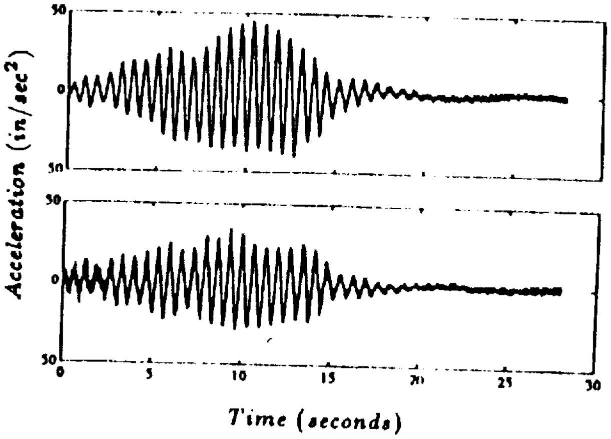

Figure 18. Closed loop responses at locations 1 and 3 with modified sensor installation

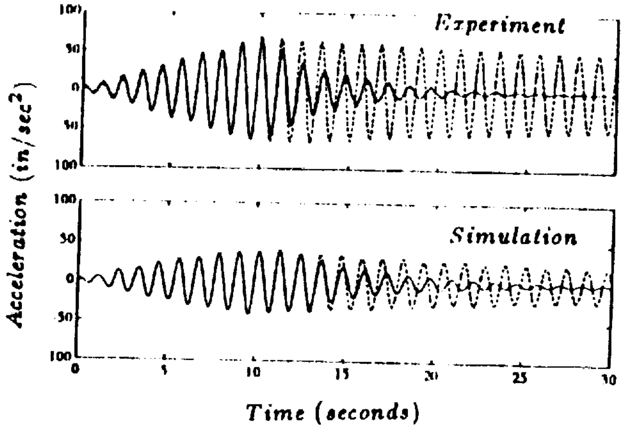

Figure 19. Open and closed loop responses at location 8 for mode 6

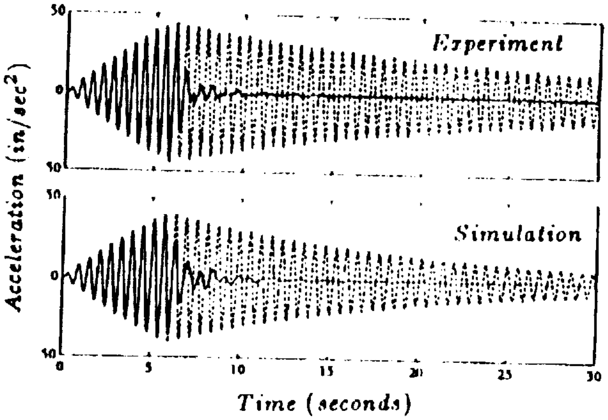

Figure 20. Open and closed-loop responses at location 2 for mode 8

ORIGINAL PAGE IS
OF POOR QUALITY

Table 3: Comparison of Experimental and Analytical Frequency and Damping Results

Mode Number	Frequency (Hz)		Damping (%)		
	Analysis	Experiment	Experiment Open-loop	Analysis Closed-loop	Experiment Closed-loop
1	.146	.14	4.7	8.7	10.6
2	.148	.14	7.0	10.9	6.8
3	.154	.15	7.0	13.0	13.5
4	.720	.73	1.5	1.5	8.2
5	.741	.72	1.2	6.5	6.2
6	.868	.90	.6	3.7	4.7
7	1.43	1.50	.4	4.6	9.3
8	1.66	1.72	.66	7.8	13.1
9	1.83	1.90	.50	4.8	8.0

Conclusions

The implementation of the active vibration absorber has been experimentally demonstrated. Using only acceleration feedback, a second order controller design is presented which represents an active tuned spring-mass-damper assembly. Experiment and simulation results show the controller performs well even in the presence of modeling errors. Since acceleration sensors are relatively inexpensive and provide an inertial measurement, this type of sensor is likely to be used in structural control applications. The controller design presented herein permits direct use of acceleration signals without the need for prefiltering. Moreover, the active vibration absorber has high stability robustness as only its performance, not its stability, is model-based. General implementation issues are discussed to insure the reader can properly use this technology in other applications. The effects of poor implementation are shown using experimental data. With proper implementation, the controller successfully augments the damping of the structure. This simple controller design, due to its high level of stability robustness, has great potential for distributed, inner- and outer-loop control systems for spacecraft structures.

References

[1] Benhabid, R.J. Flashner, H.K., and Tung, F.C., "ACOSS Fourteen (Active Control of Space Structures)," RADC-TR-83-51, Final Report, March 1983.

[2] Irwin, R.D.Jones, V.L., Rice, S.A. Tollison, D.K., and Seltzer, S.M., "Active Control Technique Evaluation for Spacecraft (ACES)", Final Report Aug. 1986-July 1987, AFWAL-TR-88-3038.

[3] Tanner, S., Pappa, R., Sulla, J., Elliott, K., Miserentino, B., Bailey, J., Cooper, P., Williams, B., "Mini-Mast CSI Testbed User's Guide," NASA TM-102630, Langley Research Center, February 1991.

[4] Belvin, W. K., Elliott, K., Bruner, A., Sulla, J. and Bailey, J., "The LaRC CSI Phase-0 Evolutionary Model Testbed: Design and Experimental Results," presented at the 4th Annual NASA/DOD Conference on Control/Structures Interaction Technology, Nov. 1990.

[5] Juang, J.-N. and Phan, M., "Robust Controller Designs for Second-Order Dynamic Systems: A Virtual Passive Approach," NASA TM-102666, Langley Research Center, May 1990.

[6] Snowdon, J.C., **Vibration and Shock in Damped Mechanical Systems**, John Wiley & Sons,Inc., New York 1968.

ORIGINAL PAGE IS
OF POOR QUALITY

NASA
National Aeronautics and Space Administration

Report Documentation Page

1. Report No.
NASA TM-104048

2. Government Accession No.

3. Recipient's Catalog No.

4. Title and Subtitle
Active Vibration Absorber for CSI Evolutionary Model:
Design and Experimental Results

5. Report Date
March 1991

6. Performing Organization Code

7. Author(s)
Anne M. Bruner, W. Keith Belvin, Lucas G. Horta, and
Jer-Nan Juang

8. Performing Organization Report No.

9. Performing Organization Name and Address
NASA Langley Research Center
Hampton, VA 23665-5225

10. Work Unit No.
590-14-61-01

11. Contract or Grant No.

12. Sponsoring Agency Name and Address
National Aeronautics and Space Administration
Washington, DC 20546-0001

13. Type of Report and Period Covered
Technical Memorandum

14. Sponsoring Agency Code

15. Supplementary Notes
Presented at the 32nd Structures, Structural Dynamics and Materials Conference
Baltimore, MD, April 8-10, 1991.
Anne M. Bruner: Lockheed Engineering & Sciences Company, Hampton, Virginia.
W. Keith Belvin, Lucas G. Horta, and Jer-Nan Juang: Langley Research Center,
Hampton, Virginia.

16. Abstract

The development of control of large flexible structures technology must include practical demonstration to aid in the understanding and characterization of controlled structures in space. To support this effort, a testbed facility has been developed to study practical implementation of new control technologies under realistic conditions. The paper discussed the design of a second-order, acceleration feedback controller which acts as an active vibration absorber. This controller provides guaranteed stability margins for collocated sensor/actuator pairs in the absence of sensor/actuator dynamics and computational time delay. Experimental results in the presence of these factors are presented and discussed. The primary performance objective considered is damping augmentation of the first nine structural modes. Comparison of experimental and predicted closed-loop damping is presented, including test and simulation and test results are not in full agreement, robustness of this design under model uncertainty is demonstrated. The basic advantage of this second-order controller design is that the stability of the controller is model independent.

17. Key Words (Suggested by Author(s))
Dissipative Controller Design
Active Vibration absorber
Control Experiments for Flexible Structures
Control-Structure Interaction

18. Distribution Statement
Unclassified--Unlimited
Subject Category 39

19. Security Classif. (of this report)	**20. Security Classif. (of this page)**	**21. No. of pages**	**22. Price**
Unclassified	Unclassified	11	A03

NASA FORM 1626 OCT 86